Annual Report of 2006 Proposal (06112):

Proposal Title: Seismic Measurements of Rock Damage and Healing on the San Andreas Fault Associated with the 2004 *M*6 Parkfield Earthquake – Toward Understanding of the Fault Behavior in Earthquake Cycle.

Proposal Category: Data Gathering and Products

Disciplinary Committee: Seismology; Fault and Rock Mechanics

Focus Group: Earthquake Source Physics

Principal Investigators: Yong-Gang Li at USC

Funding Agent: Southern California Earthquake Center.

Date: February 1, 2006 to January 31, 2007.

I. Low-Velocity Damage Zone on the San Andreas Fault at Seismogenic Depths near SAFOD Site

Under the award of EarthScope, we deployed a dense linear array of 45 seismometers across and along the San Andreas fault (SAF) near the SAFOD site at Parkfield to record fault-zone trapped waves (FZTWs) generated by near-surface explosions and microearthquakes located within the fault zone. Observations and simulations of the fault-zone trapped waves show a ~150-200-m-wide low-velocity waveguide along the SAF, within which shear velocities are reduced by 20-40% from wall-rock velocities and the *Q* value of fault-zone rocks is 10-50, indicating the existence of a damage zone on the major plate boundary at Parkfield. The damage zone on the SAF extends across seismogenic depths to at least ~7 km and is not symmetric but extends farther on the southwest side of the main fault trace. The width and velocities of this zone delineated by fault-zone trapped waves recorded at surface arrays are consistent with the results from SAFOD drilling and logs that show high porosity and multiple slip planes in a ~200-m-wide low-velocity zone with an average velocity reduction of ~20-30% on the main SAF at ~3.2 km depth [Hickman, 2005]. Recently, down-hole seismic stations within the main fault zone at this depth also registered prominent fault-zone guided waves from microearthquakes occurring below, indicating that the low-velocity waveguide on the SAF extends to the deeper seismogenic level [Ellsworth and Malin, 2006].

Data and Results

Coordinated by SAFOD PIs, we deployed a dense linear seismic array near the SAFOD site for seismic site characterization (Fig. 1). During the experiment, we recorded ~100 local earthquakes at depths between 2 and 12 km and 5 explosions detonated by the USGS. The data show prominent fault-zone trapped waves generated by the events located within the fault zone and have been used to delineate the internal damage structure and physical properties of the SAF at seismogenic depths.

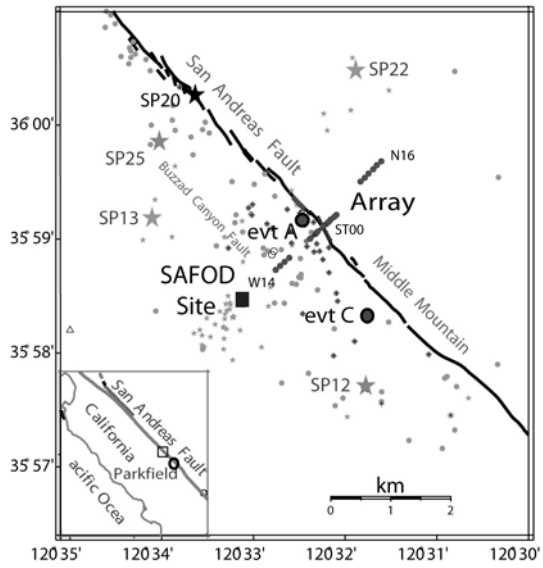

Figure 1 Map shows locations of linear seismic arrays (circles in line) deployed across and along the San Andreas fault near the SAFOD site (square), 5 explosions (stars), small shots (stars) and microearthquakes (dots) recorded at our array in the fall of 2003. Station ST0 in array was located on the main fault trace. Dark dots denote 33 earthquakes at different depths showing fault-zone trapped waves and are used for measurements shown in Fig. 3. Event A is a *M*2.2 SAFOD drilling target event occurring at ~3 km depth. Event C is a deep event at 11 km depth.

Figure 2 exhibits seismograms recorded at cross-fault array for 2 microearthquakes occurring within the fault zone at different depths near the SAFOD site, showing prominent fault-zone trapped waves (FZTW) with large amplitudes and long wavetrains after *S*-arrivals at stations close to the SAF main trace in a width range of ~150-200-m. In contrast, FZTWs are not seen clearly at stations out of this zone, but we note some seismic energy trapped within a branch fault (BF) which may connect to the main fault trace at depth. We also note that FZTWs from the deep event C at ~11 km depth show much longer wavetrains of the FZTW after S-arrivals than those generated by the SAFOD drilling target event A at ~3 km depth, indicating that the low-velocity waveguide on the SAF likely extends to deep seismogenic level.

In order to examine the depth extension of the low-velocity zone (LVZ) on the SAF, we used the data from 33 microearthquakes located within/close to the fault zone at different depths with the raypath incidence angles to the array smaller than 30^o from vertical (Fig. 3a). Figure 3b shows seismograms and envelopes at station ST0 located on the main fault trace for 11 on-fault events at different depths near SAFOD site. *S*-arrivals for these events are aligned at 2 s. The length of fault-zone trapped wavetrains following *S*-arrivals progressively increases from ~1.2 s to ~2.2 s as the event depths increase from 2.6 km to 11.7 km. In contrast, much shorter wavetrains after *S*-arrivals with flat changes in length are registered at the same station for 11 off-fault events located 1-5 km away from the fault zone in the similar depth range. In Figure 3c, we plot the measured FZTW wavetrain lengths for 33 on-fault events and 13 off-fault events at depths between 2 km and 12 km at stations located within and out of the fault zone, indicating that the low-velocity waveguide (damage zone) on the SAF extends across seismogenic depths to at least 7-8 km although the velocity reduction within the zone becomes smaller with depth due to the larger confined stress at greater depths.

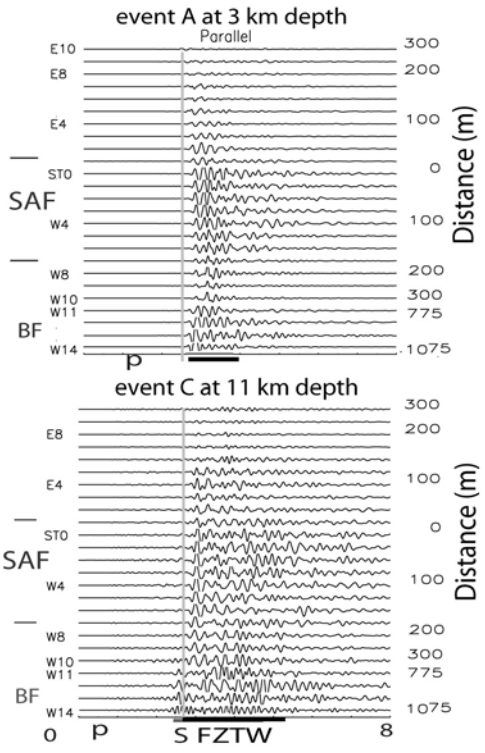

Figure 2 (a) Fault-parallel-component seismograms at the cross-fault array for 2 on-fault microearthquakes. Station names and distances from the main fault trace (SAF) are denoted. Seismograms have been (<6 Hz) filtered and plotted in a fixed amplitude scale in each plot. Prominent fault-zone trapped waves (FZTW) appear at stations between E6 and W4. *S* arrivals from these events are aligned. The solid bar denotes the length of FZTW wavetrains after *S*-waves, showing ~2.2 s duration for event C at 11 km depth and ~1.2 s duration for event A at ~3 km. Some seismic energy was trapped within a branch fault (BF) on the SW side of the SAF.

Based on our observations of fault-zone trapped waves, we construct a velocity and *Q* model across the SAF near the SAFOD site as shown in Fig. 4a. The wall-rock velocities are constrained by tomography profiles at Parkfield [*Thurber et al.*, 2003]. We have modeled these types of fault-zone trapped waves (FZTWs) waves using finite difference methods (Fig. 4c). We simulated FZTWs generated by explosions to determine the shallow 1 or 2 km fault zone structure, and then simulated trapped waves from earthquakes to obtain a model of the SAF with depth-variable structure at seismogenic depths. The model suggests that, on average, a fault zone cross section consist of a composite of two sub-vertical layers, one a 30-m-wide fault core, the other a surrounding 100-200- m-wide damage zone. The damage zone velocities range between 65-75% of the fault zone wall rocks, while those of the core are as low as 50% of the intact rock [*Li et al.*, 1990, 1997, 2004]. Down-hole seismographs emplaced in the SAFOD Main Hole at ~3 km depths also register prominent FZTWs from deeper events

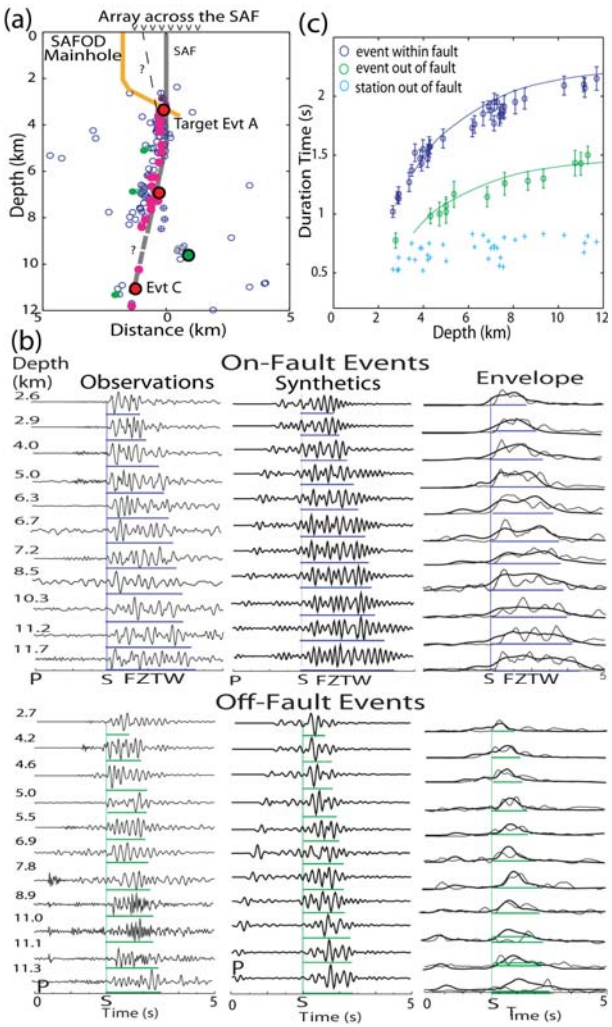

Figure 3 (a) Vertical section across the SAF and the SAFOD site shows locations of microearthquakes recorded at our seismic array in 2003. Red (green) circles denote earthquakes showing FZTWs with long (short) wavetrains after *S*-arrivals. The SAF dips toward SW slightly at depth. Waveforms from events A and C are shown in Fig. 2. The SAF and a branch fault (dashed lines) may connect at depth. (b) top: Vertical-component observed and synthetic seismograms and envelopes at station ST0 on the SAF main trace for 11 on-fault earthquakes at different depths show an increase in wavetrain length (marked by blue bars) of FZTWs as event depths increase. *S*-arrivals for the events are aligned at 2 s. Bottom: The same plot but for 11 off-fault events shows much shorter wavetrains (marked by green bars) after *S*-arrivals and flat changes with event depths. Finite-difference synthetic seismograms and envelops at station ST0 for these events using the fault-zone structural model in Fig. 4a, showing agreement between observations and synthetics. (d) The measured wavetrain lengths of FZTWs versus event depths for on- and off-fault earthquakes. Each data point is averaged from measurements at 4 stations close to or far away from the fault for on-fault. Error bars are standard deviations. Curves are polynomial fits to the data. Crosses are measurements at stations located 300-m away from the fault for all these events. Plots indicate that the low-velocity zone on the SAF extends across seismogenic depths.

[*Ellsworth and Malin*, 2006]. The width and velocity reduction of the damage zone at this depth as delineated by FZTWs has been verified by the SAFOD drilling and logs [*Hickman et al.*, 2005], showing a ~200-m-wide zone of high porosity, multiple slip planes, and average velocity reductions of ~30% with the maximum reduction of ~40% in the ~30-m-wide core zone at these depths (Fig. 4b). Thus this is the minimum depth to which the LVZ extend on the SAF at SAFOD site. In fact, observations and models of FZTWs generated by microearthquakes at different focal depths suggest that this type of fault structure reaches to depths of 6-to-7 km or more. While the velocity contrasts and layer thickness appear to become smaller with increasing depth, it is likely that a low velocity fault guided "channel" extend across the entire seismogenic depth at Parkfield. The damage zone of the SAF is not laterally symmetric. Instead, it appears to extend farther into the SW side of the fault. This could be due to rocks already weakened from previous faulting *[Chester et al.*, 1993]. It could also be due to greater damage in the extensional quadrant near the propagating crack tip of Parkfield earthquakes [*Andrews*, 2005]. We interpret the low-velocity waveguide as being a zone of accumulated damage from recurrent major earthquakes, including the 2004 *M*6 earthquake. This type of damage varies with depth and also along the strike, and may relate to the on- and near-fault variations in stress and slip distribution during earthquake rupture.

Using this fault-zone model in Fig. 4a, we simulated seismograms (Fig. 3b) at station ST0 for those on- and off-fault earthquakes at depths for comparison with observed seismograms. The lengths of synthetic FZTW wavetrains are in general agreeable with observations, further verifying that the low-velocity waveguide (damage zone) on the SAF likely extends to seismogenic depths deeper than ~7 km.

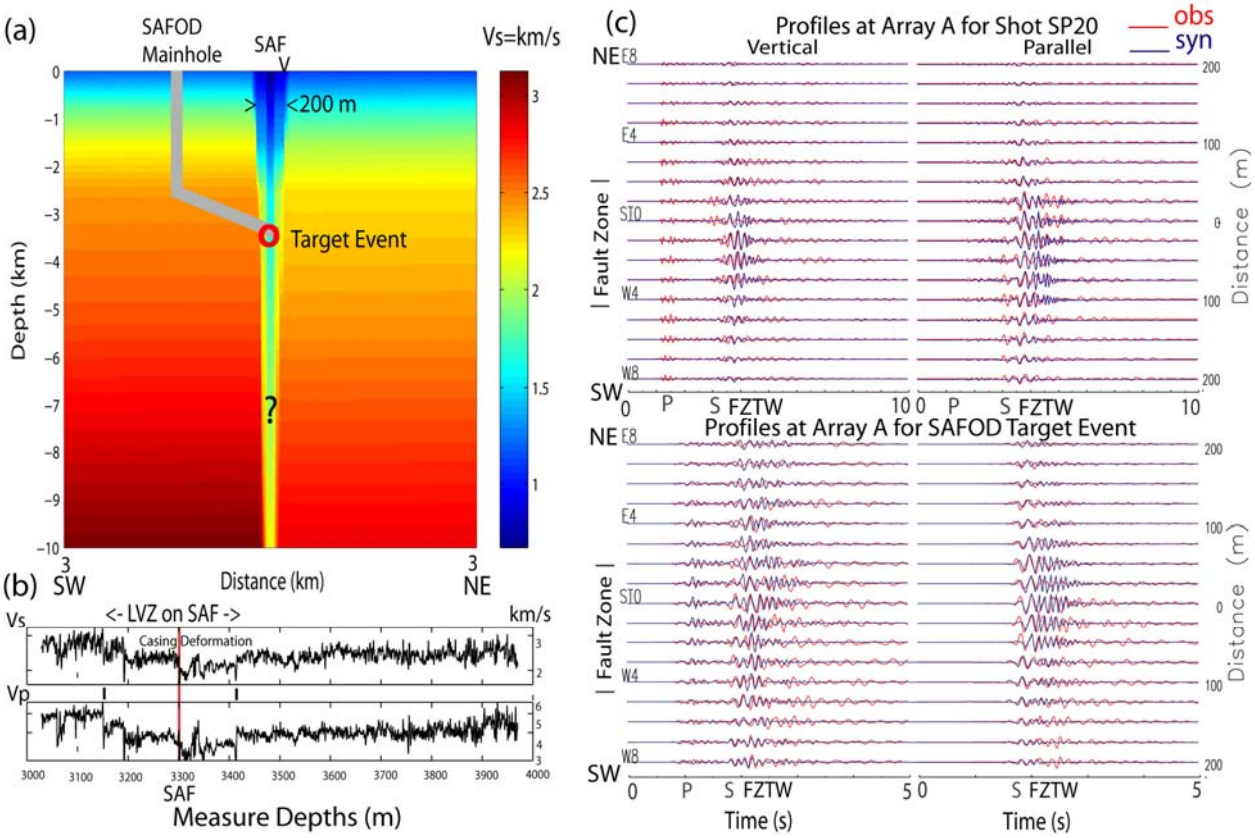

Figure 4 (a) Cross-fault depth section showing the S-wave velocity model on the SAF near the SAFOD site. The velocities within the 100-200-m-wide waveguide and surrounding rocks were found by 3-D finite-difference fits to FZTWs generated by explosions and earthquakes at different depths. The model consists of consists of two a 30 m-wide fault core and a surrounding 100-200 m wide damage zone. S velocities within the damage zone are reduced by 25-35% from surrounding-rock velocities. The maximum reduction occurs in the fault core and can be as large as 50%. The arrow indicates the surface trace of the SAF, which is offset to the NE of the fault core. (b) The width and velocity of the damage zone from fault-zone guided waves as compared to well logging velocity measurements at ~3 km (Figure from Hickman et al., 2005). Observed and 3-D finite-difference synthetic seismograms using the model in Fig. 4a for an explosion SP20 detonated within the fault zone and the SAFOD drilling target event A occurring at 3 km depth. A double-couple source is used for earthquakes while an explosion source is used for the shot.

Conclusion

The spatial extent of fault weakness, and the loss and recouping of strength across the earthquake cycle are critical ingredients in our understanding of fault mechanics. In order to relate present-day crustal stresses and fault motions to the geological structures formed in their past earthquake histories, we must understand the evolution of fault systems on many spatial and time scales. Extensive field and laboratory research, and numerical simulations indicate that fault zones undergo high, fluctuating stress and pervasive cracking during a earthquake [e.g., *Aki*, 1984; *Chester et al*., 1993]. While we know slip is localized on faults because of their lower strength compared to the surrounding bedrock, critical parameters remain unknown. For example, friction laws are approximate, and the magnitude of strength reduction and its spatial extent at seismogenic depth are still not well constrained [e.g., *Hickman and Evans*, 1992].

Our observations and modeling of fault-zone trapped waves recorded at dense linear seismic arrays deployed near the SAFOD site, Parkfield show the existence of a distinct low-velocity damage zone along the SAF and extending across seismogenic depths. The structural model for the SAF shown in Fig. 4a is still a simple one although it explains part of the data. The true structure in 3-D may be more complicated. It will be elucidated through a detailed study using the data recorded at surface and in the SAFOD main hole.

Acknowledgments. This study is supported by EarthScope Grant EAR0342277, USGS Grant NEHRP20060160, and the SCEC. Special thanks to S. Hickman, W. Ellsworth, and M. Zoback for their coordination, and E. Cochran, C. Thurber, S. Roecker, M. Rymer, R. Catchings, A. Snyder, L. Powell, B. Nadeau, N. Boness, and D. McPhee for their collaborations in our experiments at Parkfield. The author was supported by the ICDP to attend the ICDP-IODP Fault-Zone Drilling Workshop at Japan in 2006.

References

Aki, K., Asperities, barriers, characteristic earthquakes, and strong motion prediction, *J. Geophys. Res*. **89**, 5867-5872,1984.

Andrews, D. J., Rupture dynamics with energy loss outside the slip zone, *J. Geophys. Res*. 110, B01307, dio:0.1029. 2005.

Chavarria, J. A., P. E. Malin, E. Shalev, and R.D. Catchings. A look inside the San Andreas Fault at Parkfield through Vertical Seismic Profiling. *Science*, **302**, 1746-1748, 2004.

Chester F., J. Evans and R. Biegel, Internal structure and weakening mechanisms of the San Andreas fault, *JGR*. **98**, 771-786, 1993.

Ellsworth, W. L., and P. Malin, A first observation of fault zone guided PSV-waves at SAFOD and its implications for fault characteristics, EOS, Transactions, American. Geophysics Union, **87**, T23E-02, 154, 2006.

Hickman, S. H., and B. Evans, Growth of grain contacts in halite by solution-transfer: Implications for diagenesis, lithification, and strength recovery, in *Fault Mechanics and Transport Properties of Rocks*, pp. 253-280, Academic, San Diego, Cal., 1992.

Hickman, S. H., M. D. Zoback, and W. L. Ellsworth, Structure and Composition of the San Andreas fault zone at Parkfield: Initial results from SAFOD Phase 1 and 2, *EOS*, **83**, No.47, 237, 2005.

Li, Y. G., P. Leary, K. Aki, and P. Malin, Seismic trapped modes in Oroville and San Andreas fault zones, *Science*, **249**, 763-766,1990.

Li, Y. G., W. Ellsworth, C. Thurber, P. Malin, K. Aki, Observations of fault-zone trapped waves excited by explosions at the San Andreas fault California, *Bull. Seism. Soc. Am.* **87**, 210-221, 1997.

Li, Y. G., J. E., Vidale, and S. E. Cochran, Low-velocity damaged structure on the San Andreas fault at Parkfield from fault-zone trapped waves, *Geophys. Res. Lett.* **31**, L12S06, p1-5, 2004.

Thurber, C., S. Roecker, K. Roberts, M. Gold, L. Powell, and K. Rittger, Earthquake location and 3-D fault zone structure along the creeping section of the San Andreas fault near Parkfield, CA: Preparing for SAFOD, *Geophys. Res. Lett*. **30**, 1112-1115, 2003.

II. Seismic Measurements of Rock Damage and Healing on the San Andreas Fault caused by the 2004 *M*6 Parkfield Earthquake

Repeated earthquakes and explosions recorded at the San Andreas Fault (SAF) near Parkfield before and after the 2004 *M*6 Parkfield earthquake show large seismic velocity variations within a ~200-m-wide zone along the fault to depths of ~6 km. The seismic arrays were co-sited in the two experiments conducted before and after this M6 earthquake, and located in the middle of a high-slip part of the surface rupture. Waveform cross-correlations of microearthquakes recorded in 2002 and subsequent repeated events recorded a week after the 2004 *M*6 mainshock show a peak ~2.5% decrease in seismic velocity at stations within the fault zone, most likely due to the co-seismic damage of fault-zone rocks during dynamic rupture of this earthquake. The damage zone is not symmetric, instead extending farther on the southwest side of the main fault trace. Seismic velocities within the fault zone measured for later repeated aftershocks in following 3-4 months show ~1.2% increase at seismogenic depths, indicating that the rock damaged in the mainshock recovers rigidity, or heals, through time. The healing rate was not constant but largest in the earliest stage of post-mainshock. The magnitude of fault damage and healing varies across and along the rupture zone, indicating that the greater damage was inflicted and thus greater healing is observed in regions with larger slip in the mainshock. Observations of rock damage during the mainshock and healing soon thereafter are consistent with our interpretation of the low-velocity waveguide on the SAF being at least partially softened in the 2004 *M*6 mainshock, with additional cumulative effects due to recurrent rupture.

Data and Results

The *M*6 Parkfield earthquake that occurred on 28 September 2004 provides us a rare opportunity to examine the possible variations in the volume and magnitude of the low-velocity anomalies on the SAF over the earthquake cycle. After this earthquake, we deployed a dense seismic array at the same sites as used in our experiment in the fall of 2002. The data recorded for repeated explosions detonated within the SAF in 2002 and after the 2004 *M*6 Parkfield earthquake show a few percent decreases in seismic wave velocity within an ~200-m-wide zone along the fault strike at the shallow depth, most likely due to the co-seismic damage of rocks during dynamic rupture in this *M*6 mainshock [*Li et al.*, 2006]. The data from clustered aftershocks at the depth to 7 km show velocity recovery by ~1.2% within the fault zone in 3.5 months after the mainshock, indicating that the damaged rock has been healing following the mainshock. The width (~200 m) of the damage zone characterized by larger velocity changes is consistent with the low-velocity waveguide model on the SAF near Parkfield derived from fault-zone trapped waves [*Li et al.*, 1990; 1997, 2004]. In our continuous study at Parkfield, waveform cross-correlations of the data recorded at our dense linear seismic arrays for repeated microearthquakes before and after the 2004 mainshock further validate the progression of co-seismic damage and post-mainshock healing on the SAF at seismogenic depths associated with this earthquake.

Immediately after the *M*6 Parkfield, California earthquake on 28 September, 2004, we deployed 45 PASSCAL seismometers in linear arrays at the same place as our previous experiment in 2002 near Parkfield to record aftershocks (Fig. 1a). The array site was located in the middle of a high-slip part of the surface rupture in this earthquake. We culled 21 clusters of repeated events from ~800 aftershocks in our recorded data using the catalog of Northern California Seismic

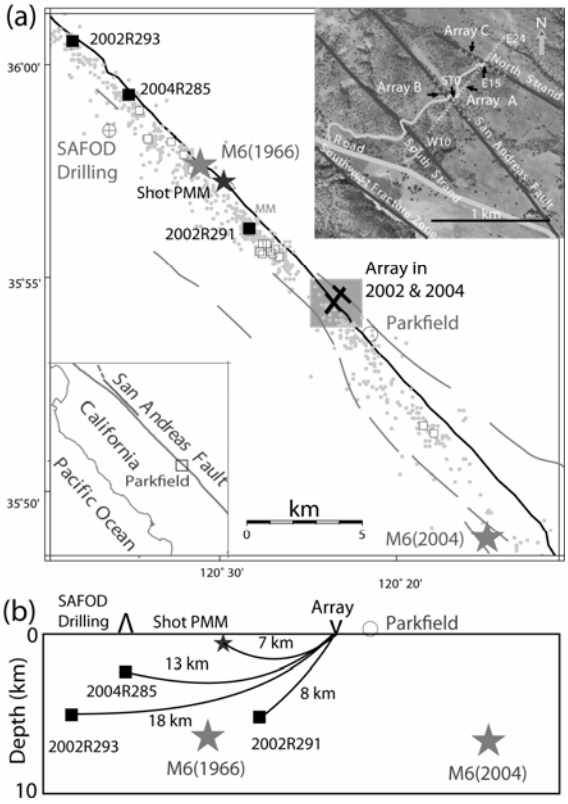

Fig. 1. (a) Map shows the location of seismic arrays (solid lines) deployed across and along the SAF near Parkfield in 2002 and 2004, repeated shot PMM (stars), microearthquakes on Julian date R291 and R293 in 2002 (solid squares) and the SAFOD target event on R285 in 2004. Dots - aftershocks of the 2004 *M*6 Parkfield earthquake. Open squares – clusters of repeated aftershocks used in our previous study for post-mainshock fault healing. Inset: Array A consists of 35 PASSCAL RT130s with station spacing of 25 m. Arrays B and C consist of 5 stations spaced at 50 m. (b) The vertical section along the SAF at Parkfield shows locations of the seismic array, shots, the 1966 and 2004 *M*6 earthquakes, and repeated events in 2002 and 2004 used in this study.

Network [R.M. Nadeau, personal communication, 2004]. Each cluster includes at least 5 repeated aftershocks occurring at the same place with the location difference among them smaller than 100 m and the difference in magnitude smaller than 0.5. Repeated aftershocks in each cluster show similar waveforms with correlation coefficient higher than 0.8. The data from clustered aftershocks have been used to examine the fault healing after the 2004 *M*6 earthquake [*Li et al*., 2006]. When we examined the data of 2004 Parkfield aftershocks, we found some clustered aftershocks occurring at the same locations of the microearthquakes recorded at our seismic array in 2002, which located beneath Middle Mountain and the SAFOD drilling site, respectively (Fig. 1b). We used the moving-window waveform cross-correlation method to measure the changes in seismic wave traveltimes for these repeated events recorded before and after the 2004 *M*6 Parkfield earthquake, and evaluate variations in velocity structure on the SAF associated with this *M*6 earthquake.

Fig. 2a shows seismograms recorded at arrays across the SAF for the event on R291 in 2002 and its repeated event on R339 in 2004, occurring within the fault zone at depth of 6 km and ~5 km northwest of the array (Fig. 1b). Prominent fault-zone trapped waves (FZTW) with relatively large amplitudes and long wavetrains following *S*-waves appeared at stations. Seismic waves traveled slower for the event after the 2004 *M*6 Parkfield earthquake. Note that stations on Array B along the main fault trace registered larger traveltime changes than those on Array C along the north fault strand (Fig. 2b). Moving-window cross-correlations of waveforms recorded for these two repeated events show ~35-65 ms delay in traveltime of dominant FZTWs between 5.5 s and 8.5 s at stations within the fault zone, but less than 20 ms delay in traveltime for the *S* waves and later coda at stations in surrounding rocks in 2004. Stations on the north fault strand registered moderate traveltime delay. In computation, we aligned the first *P*-arrivals for repeated events to avoid errors in event origin times in the catalog so the true traveltime delays for *S* and FZTWs may contain small undetermined changes in *P* traveltime. Assuming that velocity changes were uniform in the crust sampled by these waves, the shear wave velocity within the fault zone decreased by ~0.7% in average plus unmeasured changes for the *P* wave between R291 in 2002 and R339 in 2004. In contrast, the shear wave velocity in surrounding rocks decreased by <0.25% during the same time period.

Fig. 3a exhibits overlapped seismograms at stations of array A for the event on R291 in 2002 and its repeated event on R288 in 2004, which occurred 2 weeks after the *M*6 Parkfield earthquake, illuminating larger traveltime delays for the earlier event than the later repeated events. Fig. 3b shows maximum increases in traveltime at stations across the fault zone measured by moving window cross-correlation between the event

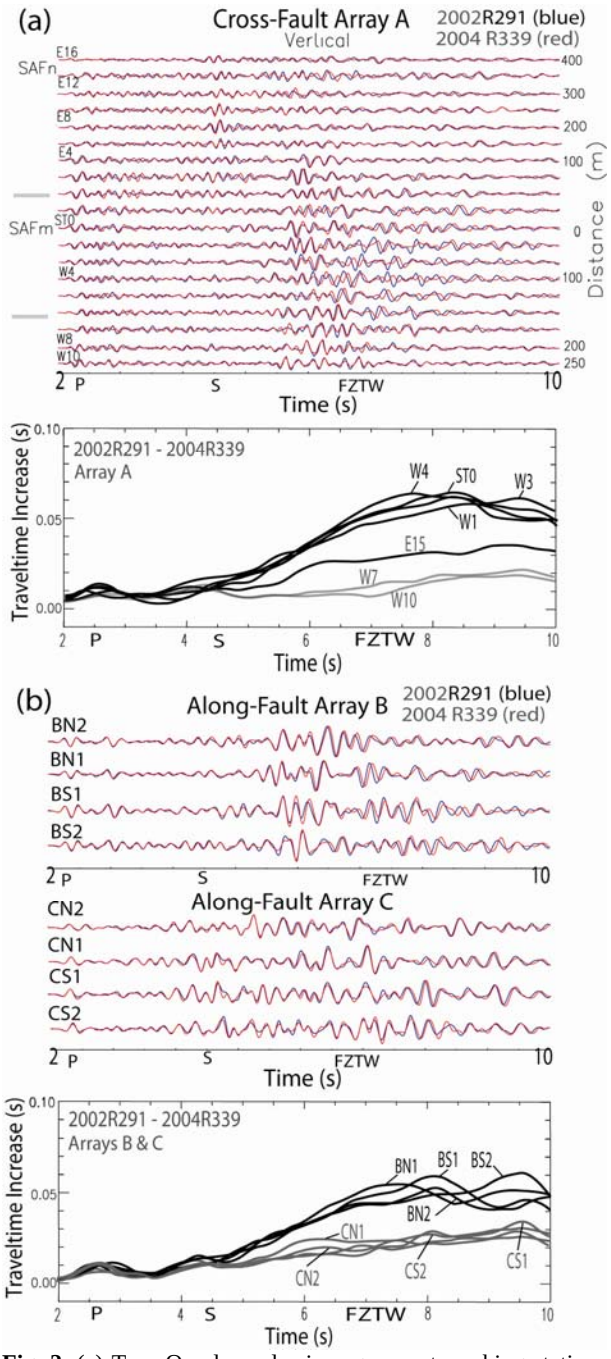

Fig. 2. (a) Top: Overlapped seismograms at working stations of Array A for the event on R291 in 2002 and its repeated event on R339 in 2004. Seismograms have been <5 Hz filtered. First *P*-arrivals from repeated events are aligned. Similar waveforms are recorded, but waves travel slower after the 2004 *M*6 Parkfield earthquake. (b) Top: Seismograms recorded at arrays B and C along the SAF main fault and north strand for these two repeated events, showing larger arrival delays at stations of array B than array C for the event in 2004. Bottom in (a) and (b): Moving-window cross-correlations of seismograms for repeated events on R291 in 2002 and on R339 in 2004 at stations of array A within and out of the fault zone, and at stations of arrays B and C, showing larger traveltime increases at stations close to the SAF main fault.

on R291 in 2002 and its repeated events on R288, R339, and R350 in 2004, showing largest traveltime delays in 2004 at stations within a ~200-m-wide zone along the main fault and much smaller changes at stations beyond this zone while intermediate changes registered at stations on the north fault strand for each pair of repeated events. We estimate that the shear wave velocity decreased by ~1.4% plus changes for *P* waves within the main fault zone between R291 in 2002 and R288 in 2004. If *P* and *S* wave velocity changes have the proportion as they would in a Poisson solid, measured traveltime increases imply that the net decrease in shear wave velocity between R291 in 2002 and R288 in 2004 was ~2.3% within the fault zone, and then recovered to a deficit of ~1.2% on R339 and R350 in 2004. Figure 3c exhibits the maximum traveltime and velocity changes measured by moving-window waveform cross-correlations at all available array stations between the event on R291 in 2002 and its 7 repeated events occurring on R288 to R350 in 2004. The data have been corrected for changes in traveltimes of *P* waves and normalized to the earliest event on R288 among them. Again, results show velocity decreases after the *M*6 Parkfield earthquake on 28 September (R273) in 2004, with the largest change of ~2.3% in a ~200-m wide zone along the SAF main trace and moderate changes at the north fault strand.

Assuming that there was no significant change in seismic velocity between the fall of 2002 and September 28, 2004 at Parkfield region, the velocity changes measured in our repeated seismic surveys are most likely associated with the September 28, 2004 *M*6 Parkfield earthquake that caused velocity decrease due to co-seismic damage of fault-zone rocks with cracks opening in dynamic rupture. The damaged rock then recovered its rigidity with time after the mainshock due to closure of cracks. We also found that the damage zone is not symmetric but extends farther on the southwest side of the main fault trace. The width of this zone characterized by largest velocity decreases caused by the recent *M*6 earthquake is consistent with the width of the low-velocity zone on the SAF delineated using FZTWs [*Li et al.*, 2004]. Observations of seismic velocity changes before and after the 2004 *M*6 Parkfield earthquake indicate that the low-velocity waveguide on the SAF has been at least partially softened, with additional cumulative damage due to recurrent ruptures. We interpret that the north strand might have experienced minor breaks due to secondary slip and strong shaking from ruptures on the main fault in major earthquakes on the SAF.

In justice to estimation of velocity variations from measured traveltime changes, we simulated seismograms for the repeated events on R291 in 2002 and on R281 in 2004 using a 3-D finite-difference code in terms of the depth-variable structure model given by *Li et al.* [2004]. Fig. 4 shows synthetic seismograms at cross-fault array and traveltime delays measured by

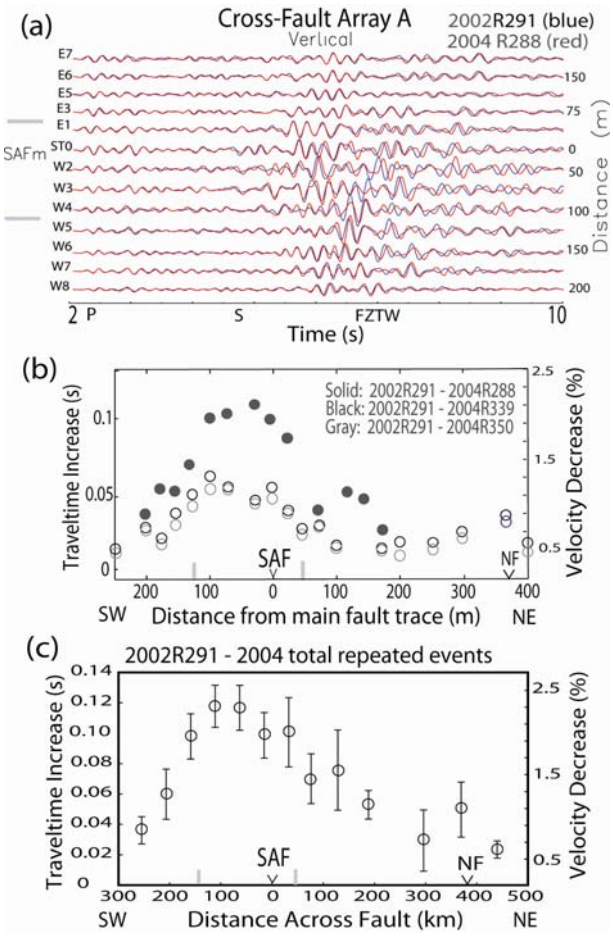

Fig. 3. (a) Overlapped seismograms at working stations of Array A for the event on R291 in 2002 and its repeated event on R288 in 2004. Seismograms have been <5 Hz filtered. (b) The maximum traveltime increases of seismic waves in 2-10 s at stations versus distances from the main fault trace measured by waveform cross-correlations between the event on R291 in 2002 and its repeated events on R288, R339 and R350 in 2004. (c) Traveltime increases and velocity decreases in percentage and standard deviations for shear wave and fault-zone trapped waves at all available stations measured by moving window cross-correlations between the event on R291 in 2002 and 6 repeated events on R288 to R350 in 2004.

moving-window cross-correlation of waveforms at stations STO and W8 within and outside of the fault zone. The synthetic traveltime delays between these repeated events are in general agreeable with observations.

In order to confirm this trend, we examined traveltime delays between the event on R291 in 2002 and its ten repeated events occurring on R281-R360, from a week to ~3.5 months after the 2004 *M*6 mainshock. Fig. 5a exhibits seismograms of these repeated aftershocks at station W1 within the fault zone, respectively. FZTWs are dominant between 7 s and 8.5 s. Waveforms for these repeated events are

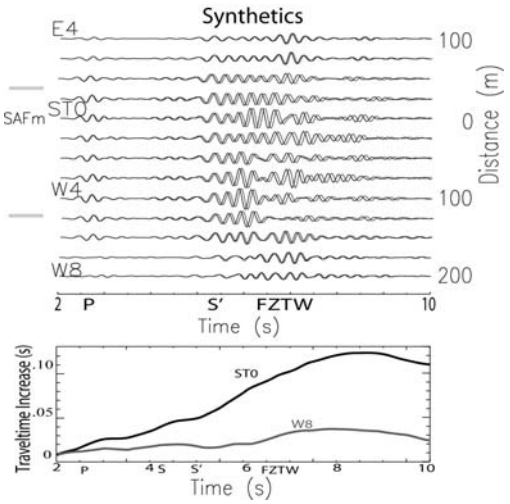

Fig. 4. top: Vertical-component of finite-difference synthetic seismograms at stations of array A for the two repeated events on R291 in 2002 (black lines) and on R281 in 2004 (gray lines) using the fault-zone model resulted from our previous experiment at this site in 2002 [*Li et al.*, 2004]. Velocities are reduced by 2.5% and 0.5% within and out of the fault-zone, respectively, for computation of seismograms for the event in 2004. Seismograms have been <5 Hz filtered. First *P*-arrivals from 2 events are aligned. bottom: Moving-window cross-correlations of seismograms for the repeated events at stations ST0 and W8 of array A within and out of the fault zone.

similar, but waves traveled faster in 2002 than in 2004. The measurements of traveltimes by moving-window cross-correlations of waveforms for repeated events show the largest delay of ~125 ms between the earliest aftershock on R281 in 2004 and the event on R291 in 2002, plus the undetermined changes of the *P*-wave (Fig. 5b). The traveltime delays gradually decreased to ~50 ms for the latest repeated event on R350, ~3 months after the 2004 mainshock. We estimate that the net shear velocity within the fault zone decreased by ~2.5% between R291 in 2002 and R281 in 2004, and then increased by ~1.2% in the following ~3 months. Although we lack of data in the first week after the 2004 Parkfield earthquake, the data recorded at our arrays indicate that shear velocities within the fault zone reduced by at least 2.5%, most likely due to the damage of fault-zone rocks in dynamic rupture of this *M*6 earthquake. The seismic velocity increases with time after the mainshock indicate that the damaged rock has being healing due to its rigidity recovery after the earthquake (Fig. 5c). The healing rate was not constant, but decreased logarithmically with time, similar to our previous observations at rupture zones of the 1992 Landers and 1999 Hector Mine earthquakes (Fig. 5d).

In our experiment at Parkfield after the 2004 *M*6 Parkfield earthquake, we recorded several small persistently repeated aftershocks on the main SAF at the location of the SAFOD "target events" (Fig. 1). Fig. 6 exhibits seismograms recorded at stations W1 located within the fault zone for these events. Waveform cross-

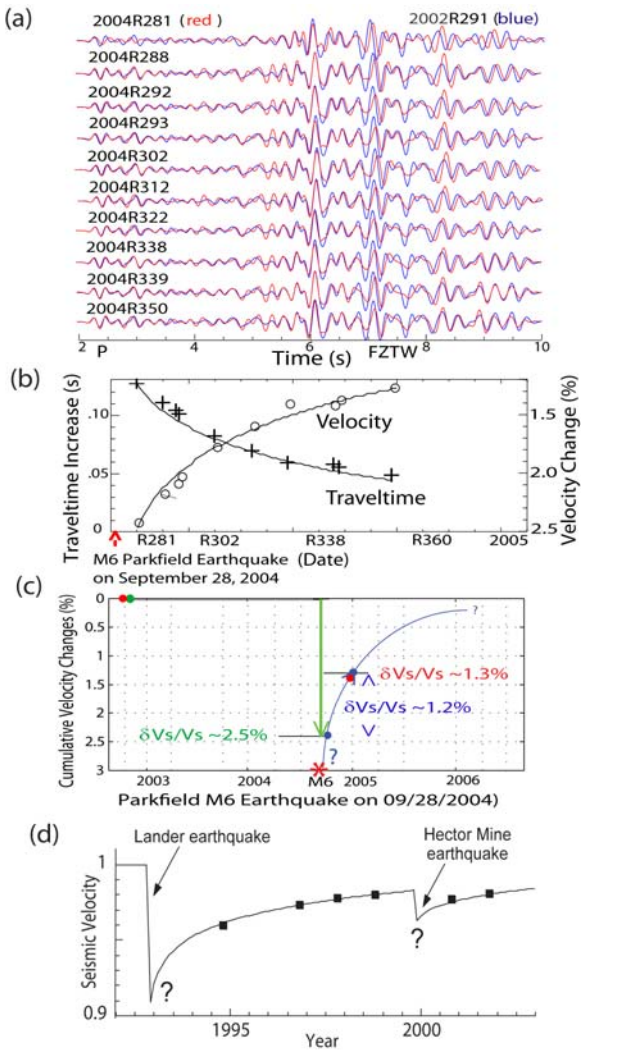

Fig. 5. (a) Vertical-component seismograms recorded at stations W1 and E7 of array A for the microearthquake on R291 in 2002 (black line) and 10 repeated events from R281 to R360 in 2004 (gray lines), showing larger traveltime increases at station W1 within the fault zone than at station E7, 175 m off the fault. Seismograms have been low-pass (<5 Hz) filtered. First *P*-arrivals from repeated events are aligned at ~2.2 s. (b) Left: Moving window cross-correlations of waveforms show traveltime increases between the event on R291 in 2002 and its 10 repeated events in 2004 with the largest increase for the earliest repeated event on R281 and a decreasing trend with dates after the mainshock. Traveltime increases are much larger at station W1 than station E7 in the same time period. Right: The maximum traveltime delays and shear velocity changes in percentage measured at stations W1 and E7 between the event on R291 in 2002 and its repeated events in 2004. The curve is the logarithmic fit to measurements of traveltime changes with a constant of velocity change 0.012 /day in logarithm. (d) The observed fault zone rock damage and healing on the SAF caused by the 2004 M6 Parkfield earthquake is consistent with the model of velocity changes as a function of time owing to combination of damage and healing at rupture zones of the 1992 M7.4 Landers and 1999 M7.1 Hector Mine earthquakes [Vidale and Li, 2003], shows healing as a logarithm of time.

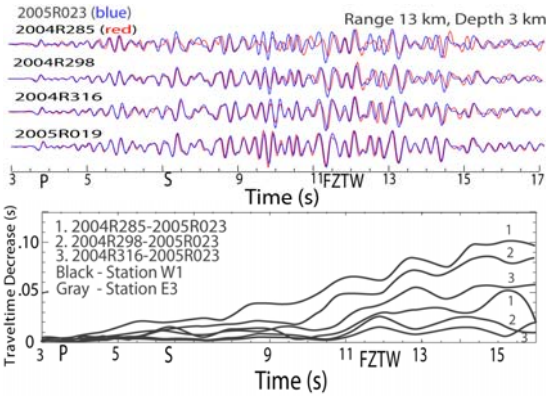

Fig. 6. Vertical-component seismograms at stations W1 within the fault zone for 5 repeated aftershocks occurring on the SAF at the location of SAFOD drilling target events at depth ~3 km. First *P*-arrivals from these events are aligned at ~3.6 s. Seismograms for the latest event on R023 in 2005 (blue line) are overlaid by those from 4 repeated aftershocks in 2004 (red lines), showing that seismic waves traveled fastest for the latest event. Waveform cross-correlations between the event on R023 in 2005 and its earlier repeated events show that travel times from these events decrease with time after the *M*6 mainshock.

correlations show that seismic waves from the latest event traveled fastest and waves from the earliest event traveled slowest, showing velocity increase with time after the *M*6 mainshock. The measured traveltime changes between the events on R023 in 2005 and R285 in 2004 is ~80 ms for guided waves plus the change for *P*-wave, showing velocity increase with fault healing after the mainshock. We estimate that the apparent shear velocity within fault zone increased by ~1.0% in ~3.5 months between R285 in 2004 and R023 in 2005, smaller than the measurements for the repeated events in the middle of a high-slip part of the surface rupture during the similar time period as shown in Fig. 5.

The measurements of traveltimes for repeated aftershocks also hint variations in magnitudes of damage and healing along the rupture zone (Fig. 7a), with greater damage-healing on the fault patch close to the 1966 *M*6 hypocenter beneath Middle Mountain where the largest dextral slip was found in the 2004 *M*6 Parkfield earthquake [*Langbein et al*., 2005]. The results from inverse of InSAR and GPS data [*Johanson et al*., 2006] show the maximum slips of ~0.5 m at depths of 4-6 km beneath Middle Mountain (Fig. 6b), correlated to the larger fault damage-healing observed in our data. Fig. 7c exhibits seismograms for 2 repeated aftershocks at 4.6 km depth, and other 2 repeated events at 9.2 km depth. The days between repeated events in the two pairs are nearly the same, but waves from the later aftershocks traveled faster than earlier events, and with larger velocity increase for the pair of deeper repeated aftershocks, indicating that the post-seismic fault healing, most likely due to the closure of cracks opened in the mainshock. The damage and healing on the SAF are most prominent above ~7 km (Fig. 7d).

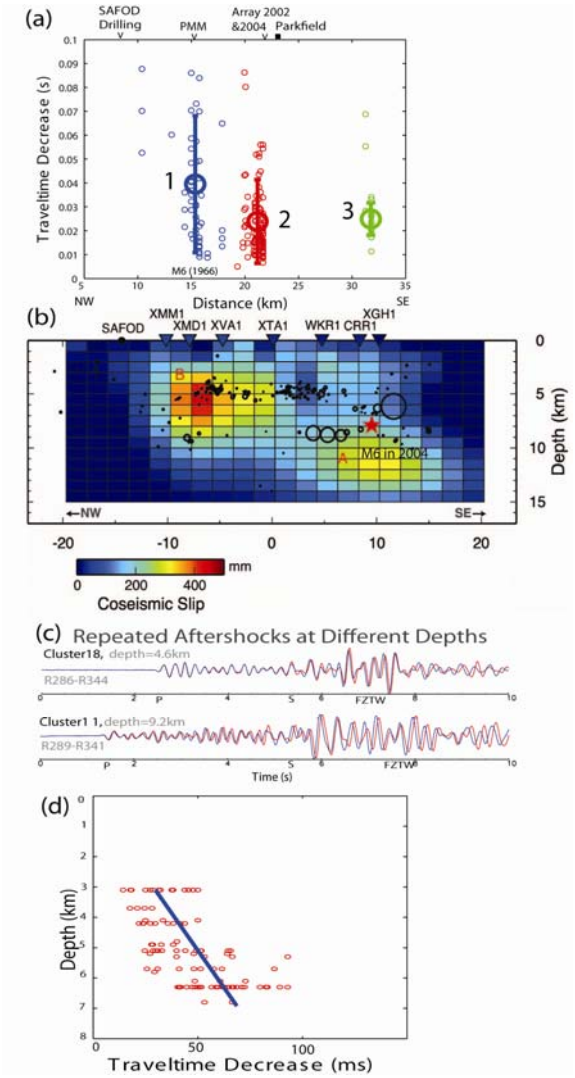

Fig. 7. (a) Traveltime decreases measured within the fault zone for 226 pairs of repeated aftershocks in 21 clusters. The measured time decreases for each pair of repeated aftershocks have been normalized to the changes in 20 days. The data are plotted versus distance along the fault strike. Mean values and standard deviations of the data for three groups of clusters are labeled by number 1, 2 and 3. Group 1 is located close to the hypocenter of the 1966 M6 earthquake. The data have been normalized to a depth range of 4 km to remove the affect of different depths of pairs on measurements. 3 groups of clusters are nearly at the same average depth. (b) Results of inversion for coseismic slip [Figure from *Johanson et al*., 2006]. The coseismic model is plotted with the first day of aftershocks. Letters A and B refer to asperities mentioned in the text. The greater damage and healing observed in our study are correlated to the larger slip. (c) Seismograms and waveform cross- correlations at a station within fault zone for 2 repeated aftershocks at 4.6 km depth and other 2 repeated events at 9.2 km depth, showing larger travel time decreases for the pair of deeper aftershocks. The data are plotted versus depths of repeated aftershocks. The straight line is the least squares fit to the data, showing that the accumulated traveltime advance increases as the event depth increases between the depth of 3 km and 7 km.

Discussion and Conclusion

In this study, we have shown the data from microearthquakes recorded at our array in October 2002 and their repeated events recorded at the same array site after the 2004 *M*6 Parkfield earthquake to determine the seismic velocity changes on the SAF at seismogenic depth before and after this earthquake using the moving-window waveform cross-correlation for these repeated events. The measurements of traveltime changes indicate a ~2.5% shear velocity decrease within the fault zone between R291 in 2002 and R281 in 2004, a week after the *M*6 Parkfield earthquake. This value is consistent with our previous estimation of the net velocity decrease on the SAF caused by this *M*6 earthquake using the data from repeated shots and clustered aftershocks [*Li et al.*, 2006]. We interpret that the 2004 *M*6 mainshock caused additional damage of rocks while the low velocity damage structure on the SAF has cumulated effects in recurrent rupture of historical earthquakes.

Our measurements of the changes in traveltime for repeated aftershocks show a ~1.2% increase in shear velocity within the rupture zone during ~3 months starting a week after the 2004 *M*6 Parkfield earthquake. It indicates that the fault heals by rigidity recovery of damaged rocks in the post-seismic stage due to the closure of cracks that opened in the mainshock. The healing rate is logarithmically decreasing through time with greater healing rate in the earlier stage of the inter-seismic period. Calculation of a ~2.5% decrease in velocity using formula for cracked media revealed that the apparent crack density within the rupture zone increased by ~0.035, which caused ~5% decrease in shear rigidity of the fault-zone rock during dynamic rupture of the 2004 *M*6 Parkfield earthquake. The subsequent 1.2% increase in *S* velocity suggests the apparent crack density within the rupture zone decreased by 0.017 in the following ~3 months.

The measurements of seismic velocity changes for repeated events occurring at different locations show variations in rock damage and healing along the fault strike, with larger magnitude in the high-slip part of the SAF beneath Middle Mountain during the 2004 *M*6 Parkfield earthquake than near the NW end of the rupture zone.

During the fault healing, the reduction of crack density may be controlled by a combination of mechanical and chemical processes on the active fault. However, the 'crack dilatancy' mechanism [*Nur*, 1972] associated with the earthquake is likely to operate for co-seismic fault damage and post-mainshock healing even if other processes are active. The stress-related temporal changes in seismic velocity caused by the 1989 Loma Prieta, California earthquake have been reported [e.g. *Baisch and Bokelmann*, 2001]. Coseismic deformation caused by this earthquake might lead to crack opening either by localizations of shear stress or by elevated pore fluid pressure. Concentrated deformation at low-strength fault zones may help to cause damage. After the earthquake, relaxation processes, such as crack healing, fluid diffusion, and post-seismic deformation cause the cracks to close again with an logarithmic recovery rate [*Dieterich*, 1972]. The variation in apparent crack density inferred by seismic velocity measurements reflects changes in either crack volume or rearrangement of aspect ratio caused by the earthquake. We tentatively conclude that the cracks that opened during the mainshock closed soon thereafter. This consistent with our interpretation of the soft low-velocity fault-zone waveguide on the SAF as being at least partially weakened in the 2004 *M*6 mainshock, but with possible significant cumulative effects as well.

Our observations of fault zone damage and healing associated with the latest *M*6 Parkfield earthquake are in general consistent with the model of velocity evolution owing to damage and healing for Lander and Hector Mine earthquakes [*Vidale and Li*, 2003]. However, the magnitude of damage and healing observed near Parkfield on the SAF is smaller than those on the Landers and Hector Mine rupture zones, probably related to the smaller magnitude mainshock, and smaller slip, and possibly differences in stress drop, pore-pressure, and rock type.

References

Baisch. S, and G. H. R. Bokelmann, Seismic waveform attributes before and after the Loma Prieta earthquake: scattering change near the earthquake and temporal recovery, *J. Geophys. Res*. **106**, 16,323-16,337, 2001.

Dieterich, J. H., Time-dependent friction in rocks, *J. Geophys. Res.* **77**, 3690-3697, 1972.

Johanson, I. A., E. J. Fielding, F. Rolandone, and R. Burgmann, Coseismic and postseismic slip of the 2004 Parkfield earthquake from space-geodetic data, *Bull. Seism. Soc. Am.* **96**, S296, 2006.

Langbein, J., R. Bocherdt, D. Dreger, J. Fletcher, J. Hardbeck, M. Hellweg, C. Ji, M. Johnston, J. Murray, R. Nadeau, M. J. Rymer, and J. Trieman . Preliminary report on the 28 September 2004, M 6.0 Parkfield, California earthquake, *Seism. Res. Lett.* **76**, 10-26, 2005.

Lees, J. M., and P. E. Malin, Tomographic images of *P* wave velocity variation at Parkfield, California, *J. Geophys. Res.* **95**, 21,793-21,804, 1990.

Li, Y. G., P. C. Leary, K. Aki, and P. E. Malin, Seismic trapped modes in Oroville & San Andreas fault zones, *Science*, **249**, 763-766, 1990.

Li, Y. G., W. L. Ellsworth, C. H. Thurber, P. E. Malin, and K. Aki, Observations of fault-zone trapped waves excited by explosions at the San Andreas fault, central California, *Bull. Seism. Soc. Am.* **87**, 210-221, 1997.

Li, Y. G., J. E., Vidale, and S. E. Cochran, Low-velocity damaged structure on the San Andreas fault at Parkfield from fault-zone trapped waves, *Geophys. Res. Lett.* **31**, L12S06, p1-5, 2004.

Li, Y. G., Po Chen, E. S. Cochran, J. E. Vidale, and T. Burdette, Seismic evidence for rock damage and healing on the San Andreas fault associated with the 2004 *M*6 Parkfield earthquake, Special issue for Parkfield *M*6 earthquake, *Bull. Seism. Soc. Am.*, **96**, pp. S1-S, doi: 10.1785/0120050803, 2006a.

Li, Y. G., P. Chen, E. S. Cochran, and J. E. Vidale, Seismic velocity variations on the San Andreas Fault caused by the 2004 *M*6 Parkfield earthquake and their implications, *Earth, Planets Space*, **58**, 1-11, 2006b.

Nur. A., Dilatancy, Pore fluid, and premonitory variations of ts/tp travel times, *Bull. Seismol. Soc. Am*. **62**, 1217-1222, 1972.

Vidale, J. E. and Li, Y. G., Damage to the shallow Landers fault from the nearby Hector Mine earthquake, Nature, 421, 524-526, 2003.

Yong-Gang Li's Bibliographic Reference During the Period of SCEC2

(January 28, 2007)

Li, Y. G., P. Chen, E. S. Cochran, and J. E. Vidale, Temporal Seismic Velocity Variations on the San Andreas Fault at Depth Caused by the 2004 M6 Parkfield Earthquake and Their Implications, Earth Planets Space, Kiyoshi Yomogida, SGEPS etc., 58, 1-11, 2006. SCEC Contribution Number **962**.

Li, Y-G, P. Chen, E. S. Cochran, J. E. Vidale, and T. Burdette, Seismic Evidence for Rock Damage and Healing on the San Andreas Fault Associated with the 2004 M6 Parkfield Earthquake, The Bulletin of Seismological Society of America, Andy Michael, Seismological Society of America, El Cerrito, V96, Parkfield Special Issue, S349-S363, 2006. SCEC Contribution Number **924**.

Cochran, E. S., Y.-G. Li and J. E. Vidale, Anisotropy in the Shallow Crust Observed around the San Andreas Fault Before and After the 2004 M 6.0 Parkfield Earthquake, Bulletin of the Seismological Society of America, V96, Parkfield Special Issue, S364–S375, 2006. SCEC Contribution Number **1080**.

Li, Y.-Gang, Vidale, John E., and Cochran, Elizabeth S., Low-Velocity Damaged Structure of the San Andreas Fault at Parkfield from Fault-Zone Trapped Waves, Geophysical Research Letters, 31, No. 12, L12S06, 1-5, 2004. SCEC Contribution Number **762**.

Vidale, J. E. and Y.-G. Li, Damage to the Shallow Landers Fault from the Nearby Hector Mine Earthquake, Nature, V421, pp. 524-526, 30 Jan., 2003. SCEC Contribution Number **1062**.

Li, Y.-G., J. E. Vidale, S. M. Day, D. D. Oglesby, E. Cochran, and Field Working Group, Post-Seismic Fault Healing on the Rupture Zone of the 1999 M7.1 Hector Mine, California Earthquake, Bulletin of the Seismological Society of America, 93, No. 2, 854-869, 2003. SCEC Contribution Number **685**.

Cochran, E. S., J. E. Vidale and Y.-G. Li, Near-fault anisotropy following the Hector Mine earthquake, Journal of Geophysical Research, V108, B9, 2436-2447, doi:10.1029/2002JB002352, 2003. SCEC Contribution Number **1081**.

Li, Y.-G. and F. L. Vernon, Characterization of the San Jacinto Fault Zone near Anza, California, from Fault-Zone Trapped Waves, Journal of Geophysical Research, 106, pp. 30,671-30,688, 2001. SCEC Contribution Number **598**.

Li, Y-G, J. E. Vidale, D. D. Oglesby, S. M. Day and E. Cochran, Multiple-Fault Rupture of the M7.1 Hector Mine, California, Earthquake from Fault-Zone Trapped Waves, Journal of Geophysical Research, 108, B3, 2165-2190, 2003. SCEC Contribution Number **596**.

Li, Y.G., and J. E. Vidale, Healing of the shallow fault zone from 1994-1998 after the 1992 M7.5 Landers, California, earthquake, Geophysical Research Letters, 28, no. 15, pp. 2999-3002, 2001. SCEC Contribution Number **552**.

Li, Y.-G., J. E. Vidale, S. M. Day, and D. D. Oglesby, Study of the 1999 M7.1 Hector Mine, California Earthquake Fault Plane by Trapped Waves, Bulletin of the Seismological Society of America, 92, No. 4, pp. 1318-1332, 2002. SCEC Contribution Number **551**.

Li, Y.G., Chester, F.M., and Vidale, J.E., Shallow Seismic Profiling at the Punchbowl Fault Zone, Southern California, Bulletin of the Seismological Society of America, 91, pp. 1820-1830, 2001. SCEC Contribution Number **507**.